Sub-Diurnal to Interannual Frequency Analysis of Observed and Modeled Reflected Shortwave Radiation from Earth

D.R. Feldman[1], W. Su[2], P. Minnis[3]

[1] Lawrence Berkeley National Laboratory, Earth and Environmental Sciences Area
[2] NASA Langley Research Center
[3] Science Systems and Applications, Inc.

Abstract:
Observational estimates of global top-of-atmosphere radiation on monthly, seasonal, annual, and longer time-scales require estimates of the diurnal variability in insolation and the asymmetry of surface and atmospheric reflection. We compare EPIC and NISTAR observations from the DSCOVR satellite with CERES hourly synoptic fluxes, which are filled through geostationary observations, and find that a Fourier analysis of these data substantially agree, showing strong relative power at sub-diurnal, diurnal, seasonal, and annual time-scales, and power growing from diurnal to seasonal time-scales. Frequency analysis of fluxes from several models shows that they distribute too much power over periods greater than 1 day but less than one year, indicating that a closer look is needed into how models achieve longer-term stability in reflected shortwave radiation. Model developers can consider using these datasets for time-varying energetic constraints, since tuning parameter choices will impact modeled planetary shortwave radiation across timescales ranging from sub-diurnal to decadal.

Submission for *Geophysical Research Letters*

Key Points:

- We present the first intercomparison of observational estimates of the Earth's albedo at sub-diurnal through inter-annual time-scales.
- These observational estimates, from CERES, EPIC, and NISTAR, are in consensus, and can therefore be used to confront models.
- Model estimates of planetary albedo show that models mostly disagree with observations at time-scales of longer than one day.

Plain-Language Summary:

The balance between incoming solar and outgoing thermal energy exerts a strong influence on the Earth's climate. The part of the incoming solar energy that is reflected back to space is called albedo. Even a slight change in albedo would dwarf the impacts of greenhouse gases, but direct observations indicate that on time-scales longer than a few years, it is remarkably stable and has been for decades. However, this albedo does fluctuate greatly at shorter time-scales, meaning that the underlying causes that ultimately shape albedo interact in a variety of ways to achieve this stability. Using novel data, we present three different observational estimates of how this reflected energy varies at these shorter time-scales, and they all substantially concur. However, a wide variety of climate models do not capture the observed variability, suggesting that further model developments is needed to better represent the underlying contributions to the Earth's albedo and the causes for its stability to date.

Keywords:

Albedo, shortwave radiative energy budget, diurnal cycle, DSCOVR

Index Terms:

1616, 1622, 1626, 1640, 1694

Introduction:

Modeling centers have recognized that the achievement of a long-term top-of-atmosphere (TOA) energy imbalance of less than 1 W/m^2 is a prerequisite that their models must achieve to produce credible historical simulations and future projections of the Earth's climate system [*Willis et al*, 2004; *Hansen et al*, 2005]. As part of the development process, model component interactions and model free parameters are tuned so that the version of each model that reports to publicly-available repositories yields results that lie within that range [*Mauritsen et al*, 2012; *Golaz et al*, 2013; *Hourdin et al*, 2017; *Schmidt et al*, 2017]. While there are other observational constraints on model tuning many of which vary from model to model, the TOA radiative tuning approach is, as far the publications to date on tuning indicate, generally consistent across models.

TOA radiative fluxes, specifically reflected shortwave and outgoing longwave radiation, are derived from NASA's Clouds and Earth's Radiant Energy System (CERES) mission [*Wielicki et al*, 1996; *Loeb et al*, 2009] and form the observational basis for model tuning. That mission directly measures broadband radiances at a fixed set of local solar hours, and from these derives best-estimates of the spatially-resolved broadband, diurnally-averaged shortwave and longwave fluxes at the TOA [*Loeb et al*, 2018]. However, there are numerous steps involved in the process chain to develop these fluxes. With respect to reflected shortwave radiation, and the associated unitless quantity of planetary albedo, some of these steps, most notably the development of diurnal averages from sun-synchronous observations, have received relatively little scrutiny.

At the same time, the importance of diurnal variability in shortwave reflection for models has long been recognized (e.g., [*Bergman and Salby*, 1997]). More recently, it was suggested that the diurnal cycle of clouds could be important to understand constraints on cloud adjustments and identify where models redistribute clouds in a warmer climate [*Webb et al*, 2015]. Over land, cloud diurnal cycles, especially, are not well-captured by models [*Yin and Porporato*, 2017]. Model errors in the diurnal cycle of cloud fraction (DCC) have been suggested to be the result of tuning the models without properly capturing the processes controlling the DCC over land [*ibid*]. Recent work has shown that Earth System Model tuning for centennial-length simulations can be developed from ensembles of 3-day model runs that better explore structural vs. parametric error [*Qian et al*, 2018], suggesting that model constraints at high frequencies are warranted.

In spite of the recognized importance of diurnal variability in reflected shortwave radiation (RSR), the lack of scrutiny of this quantity is due primarily to a lack of observational datasets that directly measure RSR across the diurnal cycle. To date, the approach has been to fill in the gaps in the diurnal cycle in direct broadband radiance observations from CERES data with geostationary observations, where the latter dataset provides high-frequency observations over a limited set of wavelengths [*Doelling et al*, 2013]. This diurnal filling has been tested with data from the Geostationary Earth Radiation Budget (GERB) mission [*Clerbaux et al*, 2009], but only over the Meteosat domain (60°S–60°N, 60°W–60°E). Global testing of the filling algorithms is warranted.

Instruments from the Deep Space Climate Observatory (DSCOVR) spacecraft provide more, and potentially complete, information about the diurnal cycle of shortwave radiation, because the spacecraft resides at the L-1 Lagrange Point between the Earth and the Sun and continuously observes almost all of the illuminated portion of the Earth from that vantage point [*Burt and Smith*, 2012; *Marshak et al*, 2018]. By virtue of DSCOVR's viewing geometry, there may be additional information about the diurnal cycle in radiative fluxes from DSCOVR beyond what has been observed previously. The DSCOVR spacecraft has two primary instruments onboard that are of direct relevance to shortwave radiation observations: the Earth Polychromatic Imaging Camera (EPIC) and the National Institute of Standards and Technology Advanced Radiometer (NISTAR). Recent work has shown how data from these instruments can be used to produce globally averaged broadband shortwave fluxes [*Su et al*, 2018; *Su et al*, 2020]. These data can be used to directly test the diurnal filling algorithms, establish the temporal structure of variability by which the Earth achieves albedo stability, and evaluate whether models capture this structure.

Here, we first compare fluxes derived from the CERES diurnal filling algorithm with fluxes derived from EPIC and NISTAR, and then evaluate the skill that models exhibit in reproducing the observed modes of variability. From these results, we conclude by discussing how high-frequency observations may be useful for model development.

Materials and Methods:

Here, we use three distinct observational datasets. First, we use the CERES Synoptic hourly shortwave radiative flux product, Edition 4.1 [*Rutan et al*, 2015]. Second, we use the hourly flux product produced from EPIC narrow-band radiances [*Su et al*, 2018], and third, we use the hourly fluxes produces from NISTAR Band-B radiances [*Su et al*, 2020]. These datasets were collected covering 2017 and 2018, and all datasets use the same angular distribution modeling (ADM) framework built from CERES [*Loeb et al*, 2003; *Su et al,* 2015]. We recognize the potential challenges of using CERES ADMs on data acquired with a substantially different viewing geometry, and will discuss implications thereof at the conclusion of this paper.

For comparing observations to models, data from the CMIP5 [*Taylor et al*, 2012] archive is used. Model radiative fluxes are taken from the Atmospheric Model Intercomparison Project (AMIP) which provides 3-hourly flux values for 1 year and includes the following models: CNRM-CM5 [*Voldoire et al*, 2013], MRI-CGCM3 [*Yukimoto et al*, 2012], and HadGEM2-ES [*Jones et al*, 2011], and 21 years for the CanESM2 model. The 3-hourly fluxes are convolved with a mask with the time-varying portion of the Earth that is within the field-of-view of the DSCOVR instrument, and this convolution is area-averaged to produce global fluxes.

We focus on observational datasets from 2017-2018, and frequency analysis is conducted on detrended flux time-series using fast Fourier Transforms. We perform discrete Fast Fourier Transforms on RSR time-series and display power spectral density (PSD) functions. For cross PSD, we use a Welch's averaged, modified periodogram method of spectral estimation (Matlab's cpsd function). Uncertainty in frequency analysis is developed using bootstrap methods, wherein we selectively remove data and determine statistical distributions for the range in power at a given frequency, assuming that spectral density power is a normally-distributed random variable [*Hall et al,* 2004].

Results:

We first present the three time-series of observationally-derived reflected shortwave radiation (RSR) from CERES SYN, EPIC, and NISTAR, shown in Figure 1(a). These data show a seasonal cycle and numerous sub-seasonal modes of variability across a wide range of time-scales, indicating that frequency analysis of these observations is warranted. Figure 1(b) presents a difference plot between the NISTAR or EPIC and CERES SYN and shows negligible differences between the EPIC and CERES SYN RSR time-series (+1.1±3.9 (1σ) W/m^2), though there are much more significant differences in fluxes between them and those from the NISTAR instrument (+11.9±7.9 (1σ) W/m^2). RSR from EPIC and NISTAR are highly correlated with the RSR from CERES SYN [*Su et al*, 2018; 2020].

The DSCOVR Science Team has investigated this RSR discrepancy and found that some of this discrepancy can be due to uncertainty in the transmission function of the filter wheel, as elaborated in *Su et al* [2020]. The differences between CERES SYN/EPIC and CERES SYN/NISTAR are plotted in Figure 1(b).

There are a number of periodic features in the RSR datasets. We will start by discussing the prominent features in observed PSDs. First, the diurnal cycle of RSR is a major feature of the time-series. It arises primarily due to the large difference in surface reflectivity between the Earth when Africa and Europe are illuminated vs. when the Pacific Ocean is illuminated. The diurnal cycles of RSR as determined from EPIC and CERES SYN fluxes are similar, as shown in Figure 1(c), while those from NISTAR are systematically higher than the other datasets due to the issues discussed above. All three datasets show similar diurnal variations. The PSDs of the three estimates of RSR are shown in Figure 1(d), normalized by the maximum power at any period, and indicate that there is substantial agreement in relative strength in modes of variability in the three time-series. There are major sources of variability at diurnal time-scales, but also secondary sources of variability at shorter periods, including at 6, 8, and 12 hours. There are also non-prominent features at periods longer than one day, for which CERES and EPIC have slightly larger disagreement. The upward slope of the PSD with period length indicates that there are a number of processes that occur at irregular intervals that contribute to variability in RSR.

Building off of the substantial agreement in the modes of variability in all-sky RSR fluxes from CERES, EPIC, and NISTAR, it is reasonable to explore the modes of variability in RSR in more detail to understand the impact of clouds on that quantity. The panels in Figure 2 indicate the contribution of clouds to the variability in RSR. Figure 2(a) shows the power spectral density function of both clear-sky and all-sky CERES SYN fluxes, where the former is estimated by calculating fluxes based on measurements of the atmospheric state, including surface albedo, aerosols, and water vapor, largely based on data from other, collocated satellites [*Rutan et al,* 2015], whereas the latter is derived from CERES radiance measurements directly. Figure 2(b) shows the cross spectral density function of clear-sky and all-sky CERES SYN fluxes and reveals, at periods of 2 hours and longer, the most prominent power at 1 day, and potentially power at seasonal time-scales. These features indicate that clouds tend to modulate and suppress the variability in RSR that would otherwise exist in the absence of clouds. That is, the more frequent occurrence of clouds over dark ocean areas reduces the albedo difference between marine and bright, relatively cloud-free land surfaces. Below seasonal time-scales, most of the modulation in variability occurs at 1-day periods, but there are non-negligible effects at sub-diurnal periods. These features are impacted by the contrast between RSR over the portion of the daylit Earth that has more land vs. RSR with more ocean. Surface albedo plays a prominent role in these sub-diurnal features, but again clouds modulate the stronger variability associated primarily with surface reflection under clear-sky conditions.

The means and 95% confidence intervals of clear- and all-sky CERES SYN PSDs, derived from observational data spanning 2001-2019, are shown in Figures 2(c) and 2(d). These plots indicate that the prominent diurnal feature of clear- and all-sky PSDs is stationary and nearly invariant over nearly 2 decades of observations. There is limited variability in sub-diurnal prominent features at 4-, 8-, and 12-hour periods of these PSDs.
Also, there are other features, such as the distribution of power between one day and several months that have an upward slope with little relative uncertainty in its upper

bound, but with no prominent features. These super-diurnal features indicate that there are a large number of interacting processes operating irregularly on super-diurnal time-scales that contribute to RSR time-series. The small level of uncertainty in features that are both super-diurnal and sub-annual suggests that these processes are stationary over time. Together, these findings indicate that there is a relatively small uncertainty in prominent features of RSR PSDs, and therefore, that comparisons between observations and model fields over a limited time-window will be meaningful and reveal underlying model skill, or lack thereof, in achieving longer-term RSR stability.

Building off of the results in Figure 2, we undertake a comparison of clear-sky and all-sky RSR PSDs between observations and models, and some results of this comparison are shown in the panels of Figure 3. They indicate that there are similarities and differences to be explored. First, the clear-sky RSR PSDs from CNRM-CM5 and HadGEM2-ES have varying levels of concurrence in their apportionment of power at diurnal and sub-diurnal 1-day periods with the CERES SYN flux product. Where models are greater than observations for sub-diurnal periods, this means that these models exhibit too much zonal contrast in RSR, and vice versa. For super-diurnal periods, the cause(s) of excessive model apportionment of power are not attributable to a single period, since the modeled power at all periods greater than one day and less than one year is greater than the observed power.

The three primary surface-atmosphere constituents that lead to clear-sky RSR variability are surface albedo, aerosols, and water vapor. Surface albedo is generally variable at super-diurnal periods, driven by changes in snow and sea-ice coverage, and to a lesser extent, changes in albedo from seasonal vegetation and surface wetness, while aerosols and water vapor can exhibit variability at sub-diurnal and super-diurnal periods. Biases in surface albedo may be due to differences in frozen surface extent and snow/ice reflectivity, but biases have also been found in modeled snow-free surface albedo [*Levine and Boos*, 2017]. However, a closer investigation regarding how these three factors interact to produce model biases is warranted to determine if the origin(s) of biases are structural, in terms of radiative transfer code issues, or parametric.

Figures 3(b) and 3(d) compare the cross-spectral density of observations and models. These figures indicate that models generally overestimate power at prominent diurnal and sub-diurnal frequencies, indicating that the variability in RSR is overly correlated between clear- and all-sky conditions in models relative to observations. That is, models overestimate how clouds modulate all-sky RSR variability relative to clear-sky RSR.

We summarize the findings of total power for clear-sky and all-sky RSR in Tables 1 and 2, respectively. The primary result that is shown by these tables is that at periods greater than 1 day but less than 1 year, models apportion too much power, indicating that they overestimate the variability in the sum of processes that contribute to albedo but have irregular periods. These findings suggest that a closer investigation into the causes of bias in the variability in modeled RSR over the range of periods from greater than 1 day to less than 1 year is warranted.

Discussion and Conclusions:

Here, we have undertaken frequency analysis of high-frequency RSR observational time-series from CERES SYN, EPIC, and NISTAR. From these observations, we have developed several findings. First, frequency analysis reveals that there are prominent sub-diurnal and diurnal features due to a zonal contrast in surface and cloud reflection, and there are no prominent features over periods greater than 1 day but less than one year, though these super-diurnal features indicate that most of the variability in RSR is contributed from a set of processes that occur at irregular intervals.

Second, we have tested whether we can use CERES SYN observations to confront Earth System Models at a range of frequencies ranging from sub-diurnal to annual. Because CERES observations at the top-of-atmosphere have few data points across the diurnal cycle, the process chain for filling in the diurnal cycle relies on geostationary products with calibration tied to MODIS. Here, we have shown that the diurnal-filling process chain, which is a key component of the development of TOA energy-balance estimates from observations, does not exhibit discernible biases, and is stationary over nearly 2 decades, so it may be considered robust for model confrontation.

More specifically, we have found that there is broad concurrence between different observational datasets, including CERES SYN, EPIC, and NISTAR on the modes of variability in the Earth's RSR. That being said, these are all predicated on radiance-to-flux conversion algorithms that have been built based on low-earth observations. It may be difficult to directly assess errors incurred in the use of these angular distribution models with such different viewing geometries, though efforts to do so have been outlined in *Su et al* [2020]. Nevertheless, where radiative transfer models indicate there is the most potential for bias in extrapolating radiance-to-flux conversion from low-earth orbit viewing geometries to those associated with L-1 orbit, targeted rotating azimuthal scans from CERES or a CERES-like instrument can be developed to constrain this conversion.

When we compare frequency features of RSR between CMIP5 models and observations, the most significant differences occur over periods ranging from greater than 1 day to less than 1 year. Both observations and models concur that there are no isolated sources of variability at regular intervals over this range of periods, but rather a number of processes that are not insignificant for RSR but occur at irregular intervals. However, the contribution to total variability over this range of periods is overestimated by models, both for clear-sky and all-sky RSR.

We also explore how clouds modulate the variability in RSR on time-scales ranging from sub-diurnal to annual, and find that over diurnal and sub-diurnal periods, models reasonably concur with observations, but, as with clear-sky RSR, models overestimate the contribution of super-diurnal frequencies to total RSR variability.

Together, these findings show that there is an uneven path by which models achieve their tuning requirement for long-term stability in reflected shortwave radiation. These high-frequency observations of shortwave flux therefore provide the model development community the opportunity to consider time-varying constraints on shortwave radiation that capture the processes by which the Earth system achieves long-term stability in albedo, and not just the long-term number. While there is no debate about the paramount importance of using tuning to ensure a model achieves TOA radiation balance in principle, the specific approaches that modeling centers have taken differ in practice. The choices in tuning this balance, which largely focus on adjusting cloud parameters, can have different temporal signatures.

We show here that there is concurrence in observational datasets in how the temporal and spatial variability of cloud systems realizes longer-term features in planetary albedo. We also show that there are significant differences between observations and models in this metric, which is disquieting. Longer-term TOA radiation balance is enforced, and therefore achieved by tuning, but there would be greater confidence in modeled radiative processes, particularly with respect to clouds, if they would substantially concur with the observations that form the basis for this radiation balance.

Especially given recent work that finds that the parametric tuning constraints, developed from perturbed-physics ensemble model simulations of 3 days, improve long-term model performance [*Qian et al*, 2018], modeling centers should, at the very least, consider using high temporal frequency features of TOA radiation as constraints in their approaches to tuning.

Acknowledgements:

This research was supported by NASA Grant NNL16AA05C. The research depended critically on NISTAR and EPIC products development made possible by the following individuals: Steve Lorentz, Alan Schwarz Yinan Yu, and Allan Smith of L-1 Standards and Technology, Inc., and David P. Duda, Konstantin Khlopenkov, and Mandana M. Thieman and Lusheng Liang of SSAI. CERES SYN data are available at https://ceres-tool.larc.nasa.gov/ord-tool/jsp/SYN1degEd41Selection.jsp. AMIP are available from https://esgf-node.llnl.gov/search/cmip5/ and EPIC and NISTAR data are available at https://tinyurl.com/yastzeo5.

Figures and Tables:

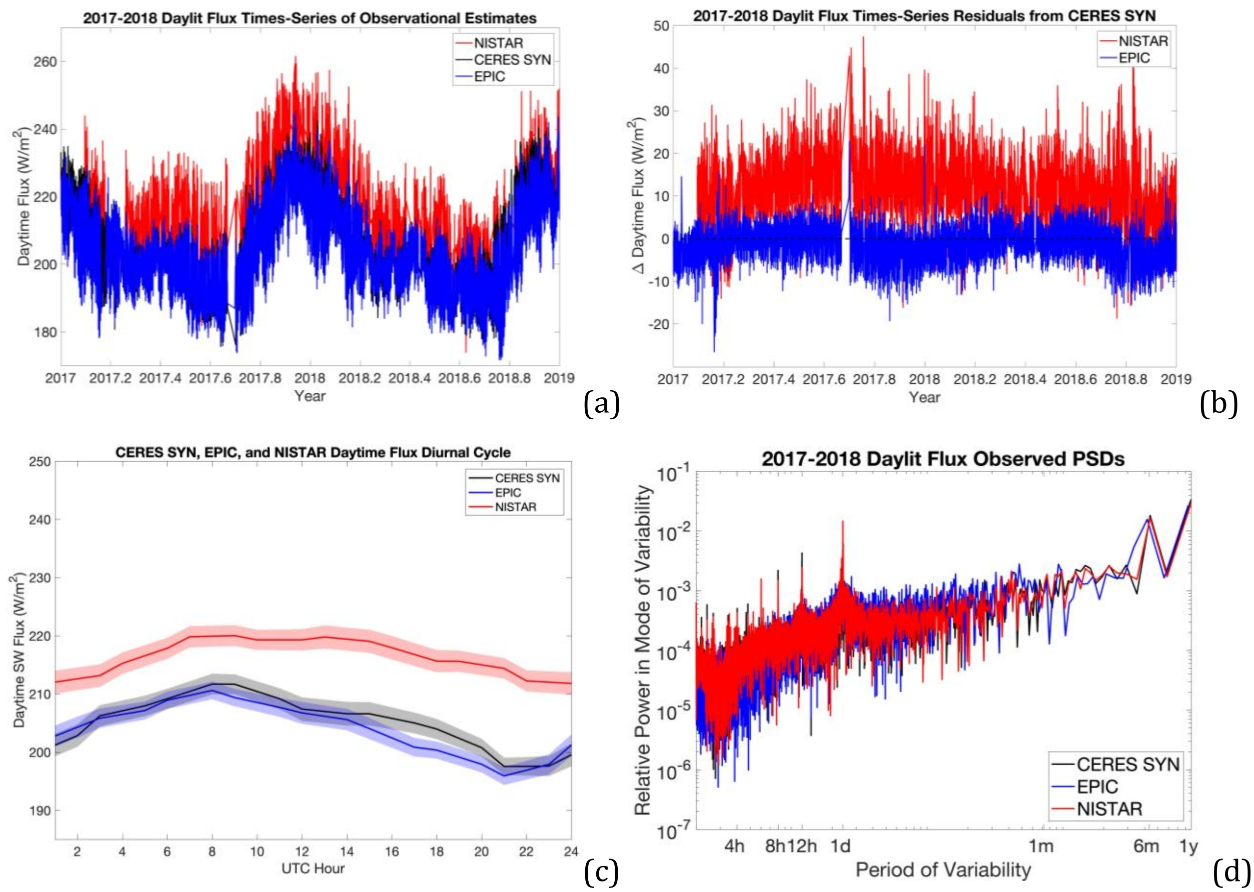

Figure 1: (a) Time-series from 2017-2019 of the daylit portion of the Earth's reflected shortwave radiation (RSR) as determined from NISTAR and EPIC Level-2 data and from the CERES SYN product. (b) Difference time-series between NISTAR or EPIC and CERES SYN RSR. (c) Diurnal cycle and 95% confidence interval from the 3 RSR data sources (d) Power spectral density of the 3 detrended RSR data sources.

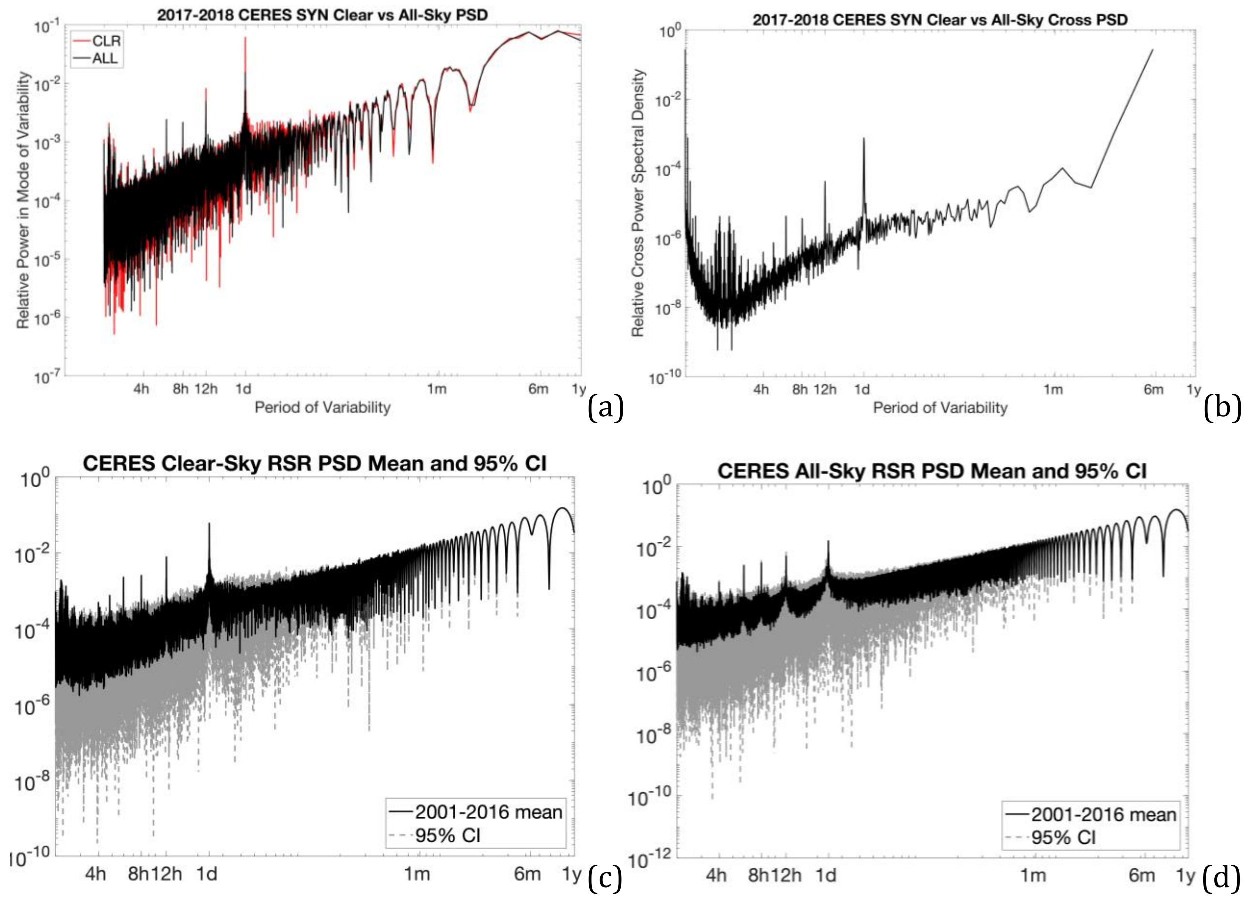

Figure 2: (a) Clear-sky (red) and all-sky (black) PSD functions of CERES SYN RSR fluxes covering 2017-2018. (b) Cross PSD function for clear-sky and all-sky CERES SYN RSR fluxes. (c) Mean and 95% confidence interval of PSD for clear-sky CERES SYN RSR fluxes derived from two-year intervals from 2001-2019. (d) Same as (c) but for all-sky CERES SYN RSR fluxes.

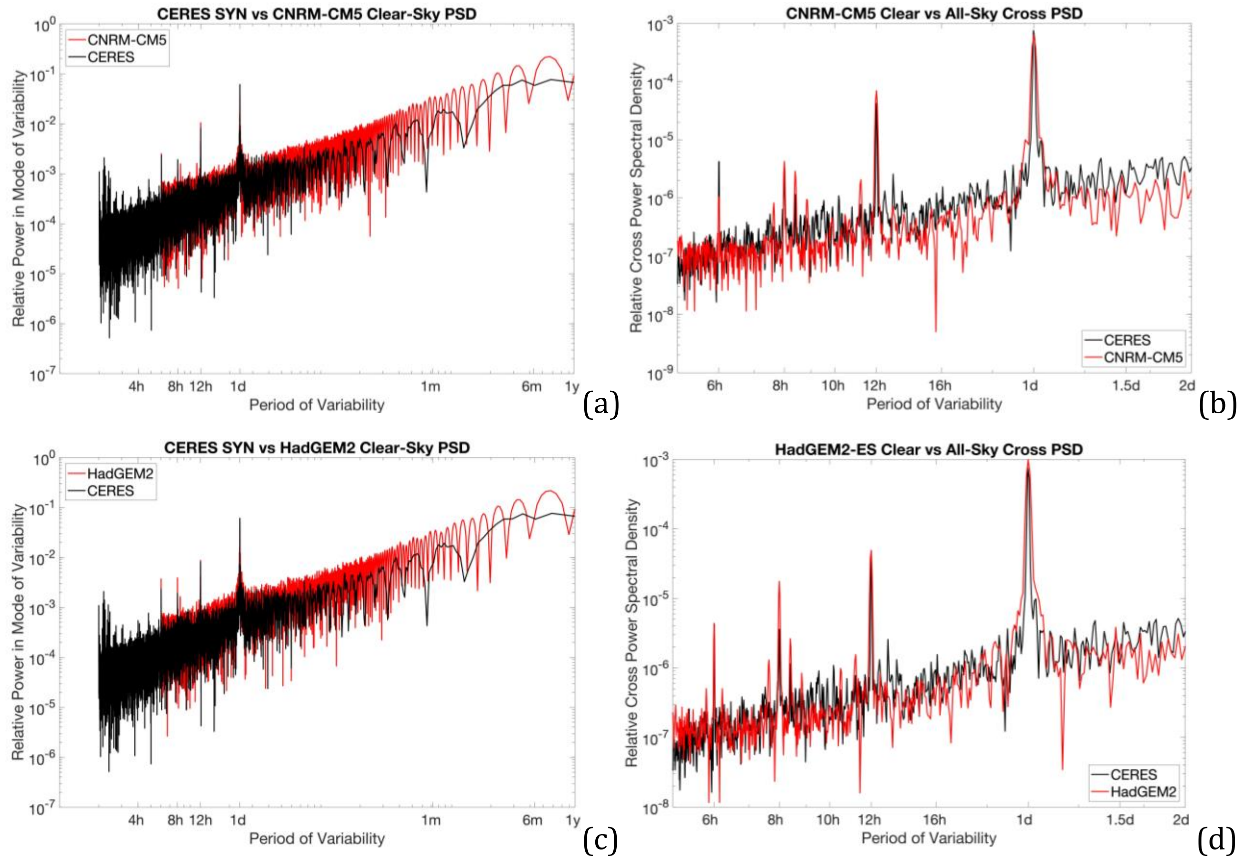

Figure 3: (a) Clear-sky RSR PSD for CERES SYN fluxes and fluxes reported by the CNRM-CM5 model. (b) Same as (a) but for clear vs all-sky cross PSD. (c) Same as (a) but for the HadGEM2-ES model.

	>1day, <1year	1 day	12 hours	8 hours
CERES SYN	0.7092 ± 0.003	0.0277 ± 1x10^{-3}	0.0088 ± 4x10^{-4}	0.005 ± 1x10^{-4}
CanAM4	0.7548	0.0328	0.0111	0.0070
CNRM-CM5	0.8020	0.0215	0.0108	0.0040
HadGEM2-ES	0.7920	0.0308	0.0096	0.0059
MRI-CGCM3	0.7781	0.0322	0.0087	0.0040

Table 1: Fraction of total power for a given period or range of periods for clear-sky daylit RSR fluxes from CERES and several AMIP models. Mean of CERES SYN represents values for 2017-2018, while uncertainty is 95% confidence interval derived all two-year intervals from 2001-2019.

	>1day, <1year	1 day	12 hours	8 hours
CERES SYN	0.5042 ± 5x10^{-3}	0.0173 ± 7x10^{-4}	0.0080 ± 2x10^{-3}	0.0070 ± 5x10^{-4}
EPIC	0.4964	0.0168	0.0118	0.0082
NISTAR	0.5879	0.0118	0.0080	0.0068
CanAM4	0.7988	0.0089	0.0066	0.0075
CNRM-CM5	0.7950	0.0101	0.0085	0.0062
HadGEM2-ES	0.8028	0.0107	0.0055	0.0072
MRI-CGCM3	0.7951	0.0128	0.0092	0.0052

Table 2: Same as Table 1, but for all-sky conditions, and including EPIC and NISTAR observations for 2017-2018.

References:

Bergman, J.W. and M.L. Salby, (1997) The Role of Cloud Diurnal Variations in the Time-Mean Energy Budget. *J. Climate,* **10**, 1114–1124, doi:10.1175/1520-0442(1997)010<1114:TROCDV>2.0.CO;2

Burt, J., R. Smith, (2012) Deep Space Climate Observatory: The DSCOVR mission, *2012 IEEE Aerospace Conference*, doi: 10.1109/AERO.2012.6187025

Clerbaux, N., et al. (2009) Comparison of GERB instantaneous radiance and flux products with CERES Edition-2 data, *Remote Sensing of Environment*, **113**, 102-114, doi:10.1016/j.rse.2008.08.016.

Doelling, D.R., N.G. Loeb, D.F. Keyes, M.L. Nordeen, D. Morstad, C. Nguyen, B.A. Wielicki, D.F. Young, and M. Sun, (2013) Geostationary Enhanced Temporal Interpolation for CERES Flux Products. *J. Atmos. Oceanic Technol.,* **30**, 1072–1090, doi:10.1175/JTECH-D-12-00136.1

Golaz, J.-C., Horowitz, L. W., and Levy, H. (2013), Cloud tuning in a coupled climate model: Impact on 20th century warming, *Geophys. Res. Lett.*, 40, 2246– 2251, doi:10.1002/grl.50232.

Hall, M.J., H.F.P. van den Boogard, R.C. Fernando, A.E. Mynett (2004) The construction of confidence intervals for frequency analysis using resampling techniques, *Hydrol. Earth Syst. Sci.*, 8, 235-246, doi:10.5194/hess-8-235-2004.

Hansen, J., et al. (2005), Earth's Energy Imbalance: Confirmation and Implications, *Science*, **308**(5727), 1431-1435, doi: 10.1126/science.1110252.

Hourdin, F., T. Mauritsen, A. Gettelman, J. Golaz, V. Balaji, Q. Duan, D. Folini, D. Ji, D. Klocke, Y. Qian, F. Rauser, C. Rio, L. Tomassini, M. Watanabe, and D. Williamson, (2017) The Art and Science of Climate Model Tuning. *Bull. Amer. Meteor. Soc.,* **98**, 589–602, doi:10.1175/BAMS-D-15-00135.1.

Jones, C.D., et al. (2011) The HadGEM2-ES implementation of CMIP5 centennial simulations, *Geosci. Mod. Dev.*, **4**, 543-570, doi: 10.5194/gmd-4-543-2011.

Levine, X. J., and Boos, W. R. (2017), Land surface albedo bias in climate models and its association with tropical rainfall, *Geophys. Res. Lett.*, 44, 6363– 6372, doi:10.1002/2017GL072510.

Loeb, N.G., N. Manalo-Smith, S. Kato, W.F. Miller, S.K. Gupta, P. Minnis, and B.A. Wielicki, (2003) Angular Distribution Models for Top-of-Atmosphere Radiative Flux Estimation from the Clouds and the Earth's Radiant Energy System Instrument on the Tropical Rainfall Measuring Mission Satellite. Part I: Methodology. *J. Appl. Meteor.,* **42**, 240–265, doi:10.1175/1520-0450(2003)042<0240:ADMFTO>2.0.CO;2

Loeb, N.G., B.A. Wielicki, D.R. Doelling, G.L. Smith, D.F. Keyes, S. Kato, N. Manalo-Smith, and T. Wong, (2009) Toward Optimal Closure of the Earth's Top-of-Atmosphere Radiation Budget. *J. Climate,* **22**, 748–766, doi:10.1175/2008JCLI2637.1.

Loeb, N.G., D.R. Doelling, H. Wang, W. Su, C. Nguyen, J.G. Corbett, L. Liang, C. Mitrescu, F.G. Rose, and S. Kato, (2018) Clouds and the Earth's Radiant Energy System (CERES) Energy Balanced and Filled (EBAF) Top-of-Atmosphere (TOA) Edition-4.0 Data Product. *J. Climate,* **31**, 895–918, doi:10.1175/JCLI-D-17-0208.1.

Marshak, A., J. Herman, S. Adam, B. Karin, S. Carn, A. Cede, I. Geogdzhayev, D. Huang, L. Huang, Y. Knyazikhin, M. Kowalewski, N. Krotkov, A. Lyapustin, R. McPeters, K.G. Meyer, O. Torres, and Y. Yang, (2018) Earth Observations from DSCOVR EPIC Instrument. *Bull. Amer. Meteor. Soc.,* **99**, 1829–1850, doi:10.1175/BAMS-D-17-0223.1

Mauritsen, T., et al. (2012), Tuning the climate of a global model, *J. Adv. Model. Earth Syst.*, 4, M00A01, doi:10.1029/2012MS000154.

Qian, Y., Wan, H., Yang, B., Golaz, J.-C., Harrop, B., Hou, Z., et al. (2018). Parametric sensitivity and uncertainty quantification in the version 1 of E3SM atmosphere model based on short perturbed parameter ensemble simulations. *Journal of Geophysical Research: Atmospheres*, **123**, 13,046– 13,073, doi:10.1029/2018JD028927.

Rutan, D.A., S. Kato, D.R. Doelling, F.G. Rose, L.T. Nguyen, T.E. Caldwell, and N.G. Loeb, (2015) CERES Synoptic Product: Methodology and Validation of Surface Radiant Flux. *J. Atmos. Oceanic Technol.,* **32**, 1121–1143, doi:10.1175/JTECH-D-14-00165.1.

Schmidt, G.A., D. Bader, L.J. Donner, G.S. Elsaesser, J.-C. Golaz, C. Hannay, A. Molod, R. Neale, S. Saha (2017) Practice and philosophy of climate model tuning across six U.S. modeling centers, *Geosci. Mod. Dev.*, 10(9), 3207-3223, doi: 10.5194/gmd-10-3207-2017.

Stephens, G. L., O'Brien, D., Webster, P. J., Pilewskie, P., Kato, S., and Li, J. (2015), The albedo of Earth. *Rev. Geophys.*, **53**, 141– 163. doi: 10.1002/2014RG000449.

Su, W., J. Corbett, Z. Eitzen, L. Liang (2015) Next-generation angular distribution models for top-of-atmosphere radiative flux calculation from CERES instruments: methodology, *Atmos. Meas. Tech.*, **8**, 611-623, doi: 10.5194/amt-8-611-2015.

Su, W., Liang, L., Doelling, D. R., Minnis, P., Duda, D. P., Khlopenkov, K. V., et al. (2018). Determining the shortwave radiative flux from Earth polychromatic imaging camera. *Journal of Geophysical Research: Atmospheres*, **123**, 11,479– 11,491. doi:10.1029/2018JD029390.

Su, W., P. Minnis, L. Liang, D.P. Duda, K. Khlopenkov, M.M. Thieman, Y. Yu, A. Smith, S. Lorentz, D. Feldman, F.P.J. Valero (2020) Determining the Daytime Earth Radiative Flux from National Institute of Standards and Technology Advanced Radiometer (NISTAR) Measurements, *Atmos. Meas. Tech. Discuss.*, doi:10.5194/amt-2019-214.

Taylor, K. E., R. J. Stouffer, and G. A. Meehl, (2012) An overview of CMIP5 and the experiment design. *Bull. Amer. Meteor. Soc.*, **93**, 485–498, doi:10.1175/BAMS-D-11-00094.1.

Trenberth, K. E., Zhang, Y., Fasullo, J. T., and Taguchi, S. (2015), Climate variability and relationships between top-of-atmosphere radiation and temperatures on Earth. *J. Geophys. Res. Atmos.*, **120**, 3642– 3659. doi: 10.1002/2014JD022887.

Voldoire, A., Sanchez-Gomez, E., Salas y Mélia, D. et al. (2013) The CNRM-CM5.1 global climate model: description and basic evaluation, *Clim Dyn,* **40**, 2091-2121, doi: 10.1007/s00382-011-1259-y.

Webb, M., et al. (2015) The diurnal cycle of marine cloud feedback in climate models, *Climate Dynamics*, 44(5-6), 1419-1436, doi:10.1007/s00382-014-2234-1

Wielicki, B.A., B.R. Barkstrom, E.F. Harrison, R.B. Lee, G.L. Smith, and J.E. Cooper, (1996) Clouds and the Earth's Radiant Energy System (CERES): An Earth Observing System Experiment. *Bull. Amer. Meteor. Soc.,* **77**, 853–868, doi:10.1175/1520-0477(1996)077<0853:CATERE>2.0.CO;2

Willis, J. K., Roemmich, D., and Cornuelle, B. (2004), Interannual variability in upper ocean heat content, temperature, and thermosteric expansion on global scales, *J. Geophys. Res.*, **109**, C12036, doi:10.1029/2003JC002260.

Yin, J., and A. Porporato (2017) Diurnal cloud cycle biases in climate models, *Nature Communications*, 8, 2269, doi: 10.1038/s41467-017-02369-4.

Yukimoto, S. et al. (2012) A New Global Climate Model of the Meteorological Research Institute: MRI-CGCM3, *Journal of the Meteorological Society of Japan*, 90A, 23-64, doi: 10.2151/jmsj.2012-A02.